

Supporting Information - Adsorptive Capacity and Evolution of the Pore Structure of Alumina on Reaction with Gaseous Hydrogen Fluoride.

Grant J. McIntosh, Gordon E. K. Agbenyegah, Margaret M. Hyland, and James B. Metson.

Contents

Section A. Full Model Results Employing the Harkins-Jura Statistical Thickness Model	3
<i>Section A1. Monolayer-only Results (Section 4.1 in Published Manuscript) – Harkins-Jura model</i>	3
Figure S1: PSD curves of a) unimodal and b) bimodal aluminas after industrial fluorination, and c) unimodal and d) bimodal samples after laboratory fluorination with the monolayer-only model. These results supplement the material presented in Section 4.1 in the published manuscript. PSD curves are generated using the Harkins-Jura statistical thickness models.	3
<i>Section A2. Monolayer/Three-Zone Model Results (Section 4.2 in Published Manuscript) – Harkins-Jura model</i>	4
Figure S2: PSD curves of a) unimodal and b) bimodal aluminas after industrial fluorination, and c) unimodal and d) bimodal samples after laboratory fluorination with the monolayer/three zone model. These results supplement the material presented in Section 4.2 in the published manuscript. PSD curves are generated using the Harkins-Jura statistical thickness models.	4
Table S1: Fitting Parameters in the ‘Monolayer Formation, Kinetic Inaccessibility, and Blocking of Fine Mesopores’ Model (using the Harkins-Jura thickness model).	4
Section B. Full Model Results Employing the Halsey Statistical Thickness Model	5
<i>Section B1. Monolayer-only Results (Section 4.1 in Published Manuscript) – Halsey model</i>	5
Figure S3: PSD curves of a) unimodal and b) bimodal aluminas after industrial fluorination, and c) unimodal and d) bimodal samples after laboratory fluorination with the monolayer-only model. These results supplement the material presented in Section 4.1 in the published manuscript. PSD curves are generated using the Halsey statistical thickness models.	5
<i>Section B2. Monolayer/Three-Zone Model Results (Section 4.2 in Published Manuscript) – Halsey model</i>	6
Figure S4: PSD curves of a) unimodal and b) bimodal aluminas after industrial fluorination, and c) unimodal and d) bimodal samples after laboratory fluorination with the monolayer/three zone model. These results supplement the material presented in Section 4.2 in the published manuscript. PSD curves are generated using the Halsey statistical thickness models.	6
Table S2: Fitting Parameters in the ‘Monolayer Formation, Kinetic Inaccessibility, and Blocking of Fine Mesopores’ Model (using the Halsey thickness model). Due to poor fits, Bimodal Laboratory results were not re-modelled.	6

<i>Section B3. Pore Attenuation/Three-Zone Model Results (Section 4.3 in Published Manuscript) – Halsey model</i>	7
-------------------------------------------------------------------------------------------------------------------------	---

Figure S5: PSD curves of a) unimodal and b) bimodal aluminas after industrial fluorination, and c) unimodal and d) bimodal samples after laboratory fluorination with the pore attenuation/three zone model. These results supplement the material presented in Section 4.3 in the published manuscript. PSD curves are generated using the Halsey statistical thickness models. 7

Table S3: Fitting parameters for the models of pore attenuation in the studied aluminas (using the Halsey thickness model). 7

Section C. Rebinning Procedure for Monolayer Application in the ‘Monolayer/Three-Zone’ Model	8
-----------------------------------------------------------------------------------------------------------	---

Section A. Full Model Results Employing the Harkins-Jura Statistical Thickness Model

This section presents full model results employing the equivalent models are presented in the published manuscript. In particular, the Harkins-Jura model of statistical thickness is employed.

Section A1. Monolayer-only Results (Section 4.1 in Published Manuscript) – Harkins-Jura model

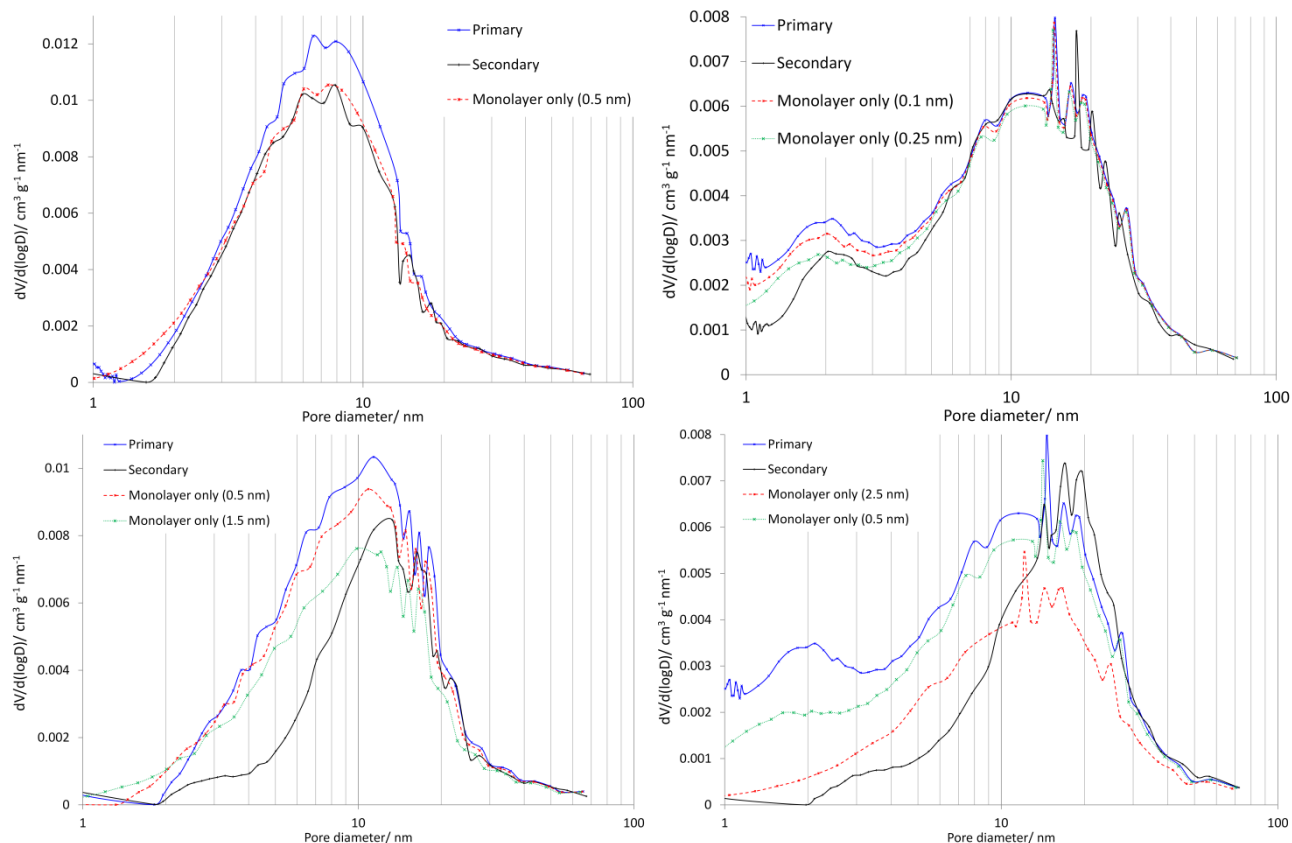


Figure S1: PSD curves of a) unimodal and b) bimodal aluminas after industrial fluorination, and c) unimodal and d) bimodal samples after laboratory fluorination with the monolayer-only model. These results supplement the material presented in Section 4.1 in the published manuscript. PSD curves are generated using the Harkins-Jura statistical thickness models.

Section A2. Monolayer/Three-Zone Model Results (Section 4.2 in Published Manuscript) – Harkins-Jura model

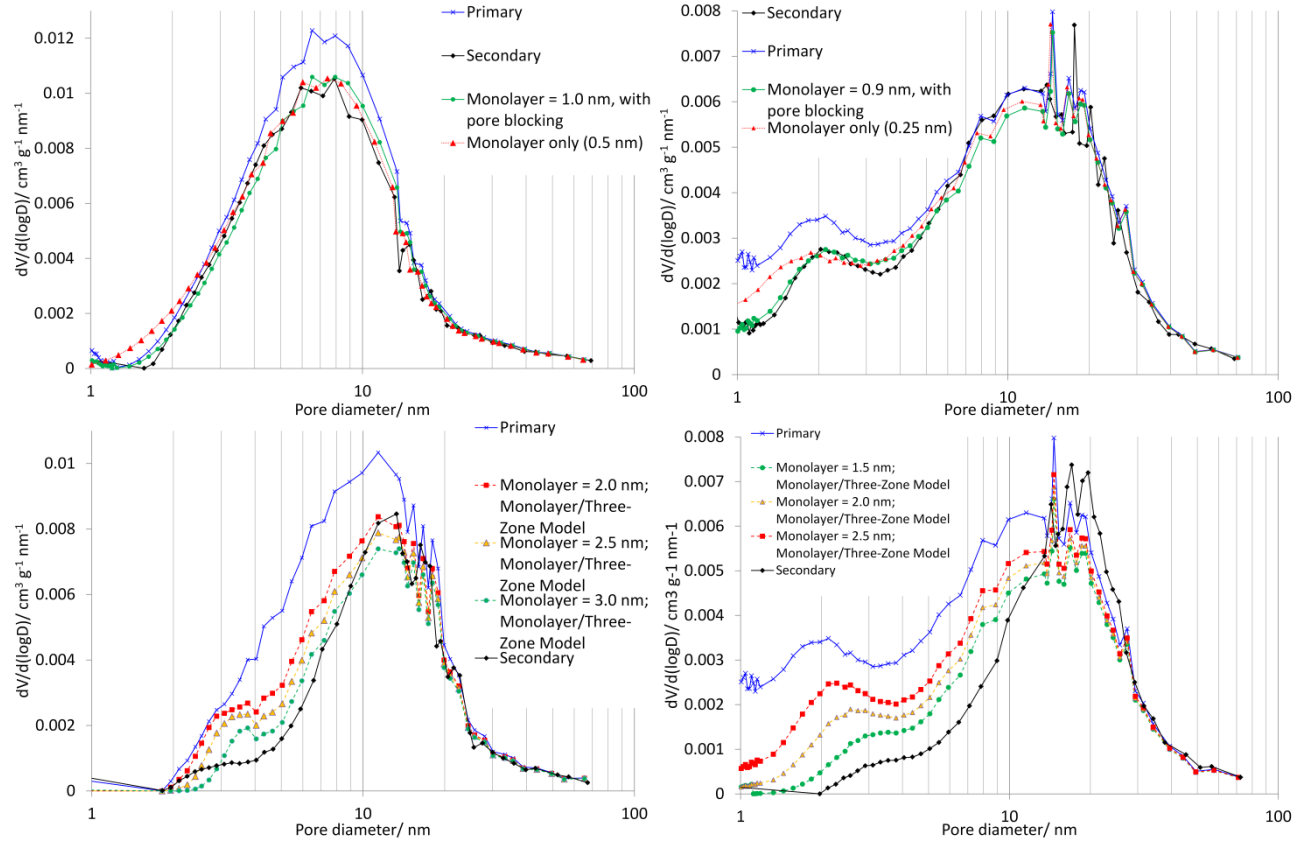


Figure S2: PSD curves of a) unimodal and b) bimodal aluminas after industrial fluorination, and c) unimodal and d) bimodal samples after laboratory fluorination with the monolayer/three zone model. These results supplement the material presented in Section 4.2 in the published manuscript. PSD curves are generated using the Harkins-Jura statistical thickness models.

Table S1: Fitting Parameters in the ‘Monolayer Formation, Kinetic Inaccessibility, and Blocking of Fine Mesopores’ Model (using the Harkins-Jura thickness model).

	Unimodal industrial	Bimodal industrial	Unimodal laboratory ^a	Unimodal laboratory ^b
D_{kinetic}	3	3.2	3.5	3
σ_{kinetic}	1	8	0.5	0.9
D_{blocked}^c	1	0.9	x	x
σ_{blocked}	1.5	0.6	0.4	0.7
t_m / nm	1	0.9	x	x

^a $x = 2.0, 2.5$, or 3.5 ; see Figure S2c.

^b $x = 1.5, 2.0$, or 2.5 ; see Figure S2d.

^c Fitting was performed assuming D_{blocked} and t_m were identical; relaxing this criterion did not improve model fitting results.

Section B. Full Model Results Employing the Halsey Statistical Thickness Model

The results presented in this section duplicate all use the Halsey equation (Halsey, G., Physical Adsorption on Non-Uniform Surfaces. *J. Chem. Phys.* 1948, 16, 931-937) for the calculation of the thickness of adsorbate lost from open pores during a given desorption step:

$$t_i = 3.54 \left(\frac{5}{\ln \left(\frac{P_0}{P_i} \right)} \right)^{\frac{1}{3}} \quad (\text{S1})$$

Section B1. Monolayer-only Results (Section 4.1 in Published Manuscript) – Halsey model

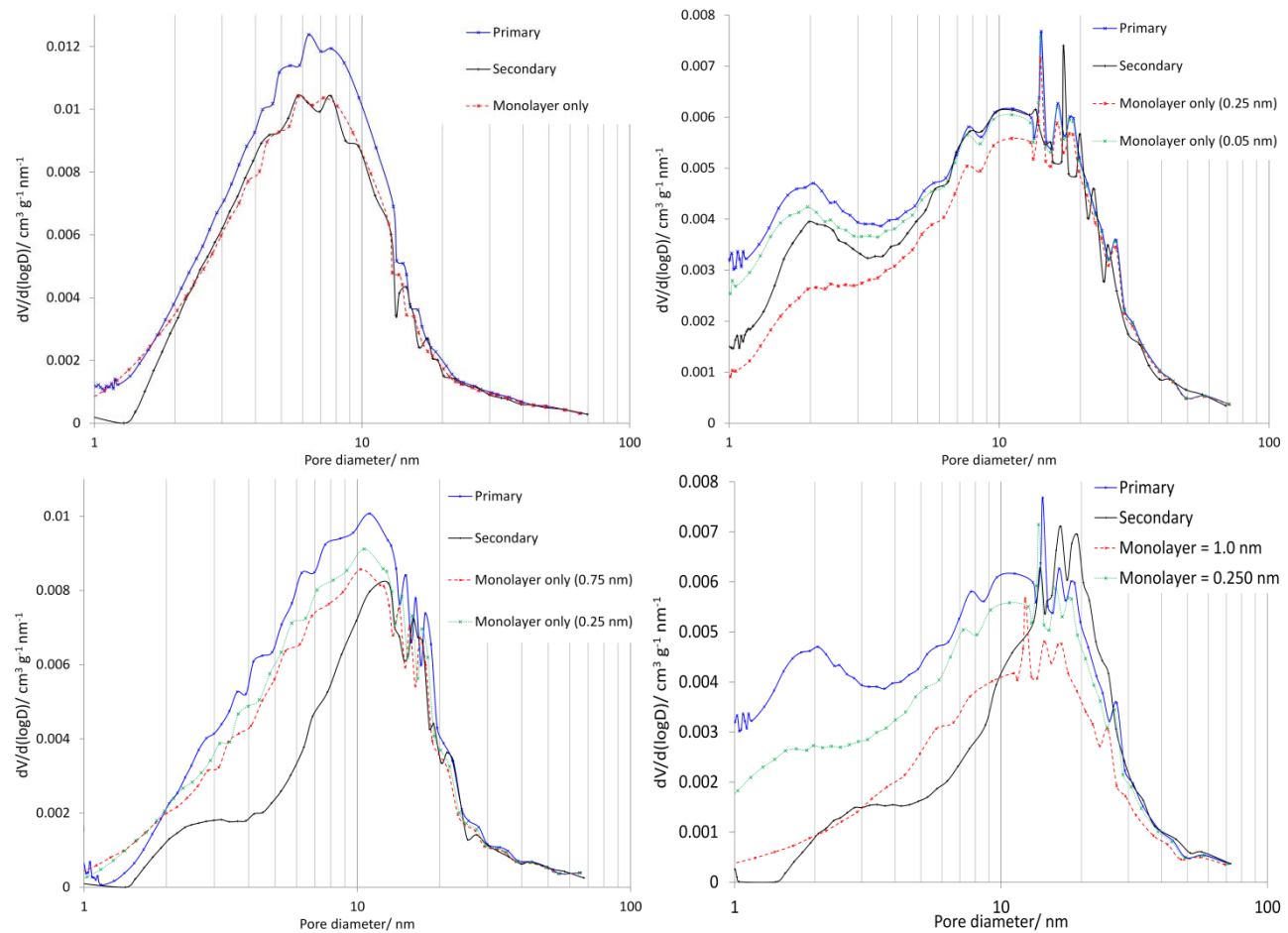


Figure S3: PSD curves of a) unimodal and b) bimodal aluminas after industrial fluorination, and c) unimodal and d) bi-modal samples after laboratory fluorination with the monolayer-only model. These results supplement the material presented in Section 4.1 in the published manuscript. PSD curves are generated using the Halsey statistical thickness models.

Section B2. Monolayer/Three-Zone Model Results (Section 4.2 in Published Manuscript) – Halsey model

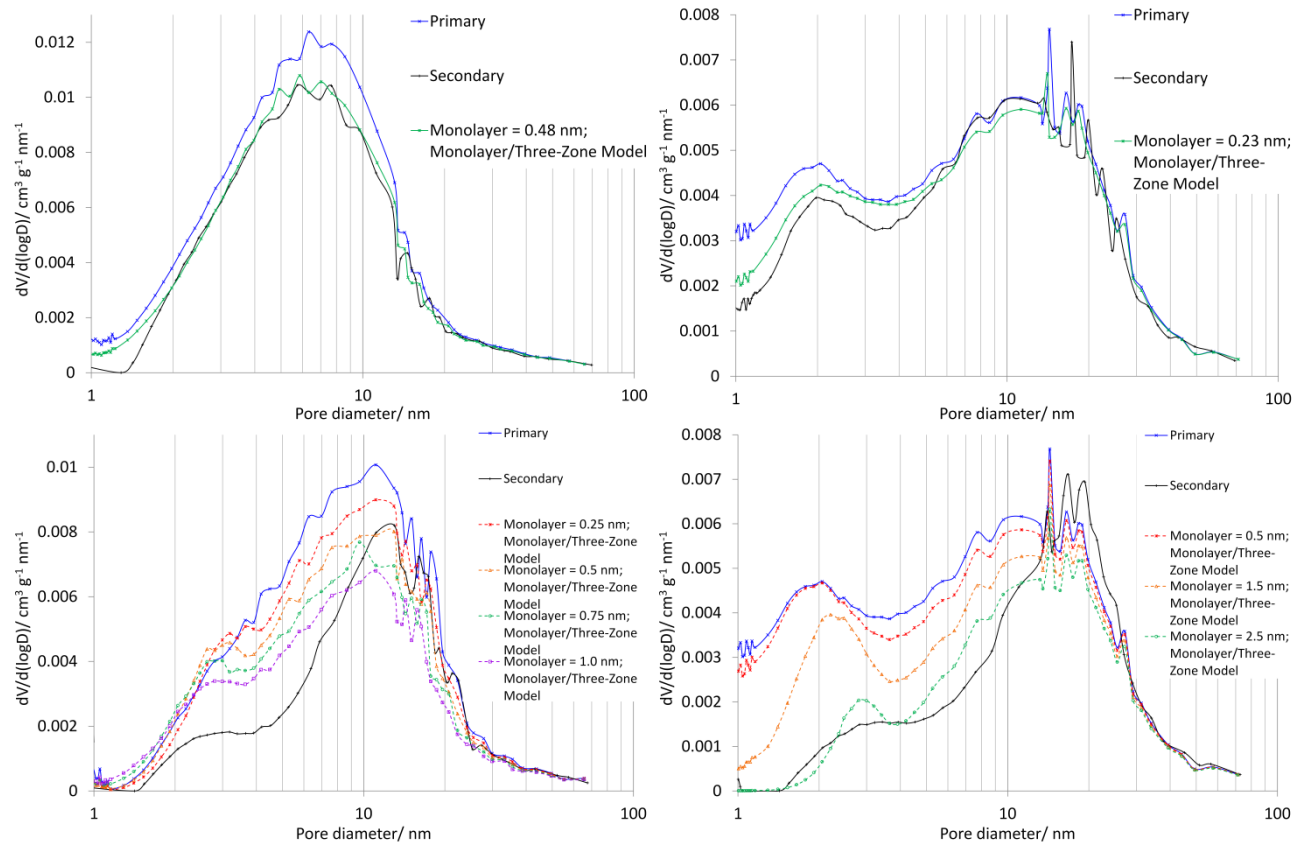


Figure S4: PSD curves of a) unimodal and b) bimodal aluminas after industrial fluorination, and c) unimodal and d) bi-modal samples after laboratory fluorination with the monolayer/three zone model. These results supplement the material presented in Section 4.2 in the published manuscript. PSD curves are generated using the Halsey statistical thickness models.

Table S2: Fitting Parameters in the ‘Monolayer Formation, Kinetic Inaccessibility, and Blocking of Fine Mesopores’ Model (using the Halsey thickness model). Due to poor fits, Bimodal Laboratory results were not re-modelled.

	Unimodal industrial	Bimodal industrial	Unimodal laboratory ^a	Bimodal laboratory ^b
D_{kinetic}	3	3	3	3
σ_{kinetic}	2	1	0.5	0.5
D_{blocked}^c	0.48	0.23	x	x
σ_{blocked}	3.2	1.5	3	0.5
t_m / nm	0.48	0.23	x	x

^a $x = 0.25, 0.5, 0.75$, or 1.0 ; see Figure S4c.

^b $x = 0.5, 1.5$, or 2.5 ; see Figure S4d.

^c Fitting was performed assuming D_{blocked} and t_m were identical; relaxing this criterion did not improve model fitting results.

Section B3. Pore Attenuation/Three-Zone Model Results (Section 4.3 in Published Manuscript) – Halsey model

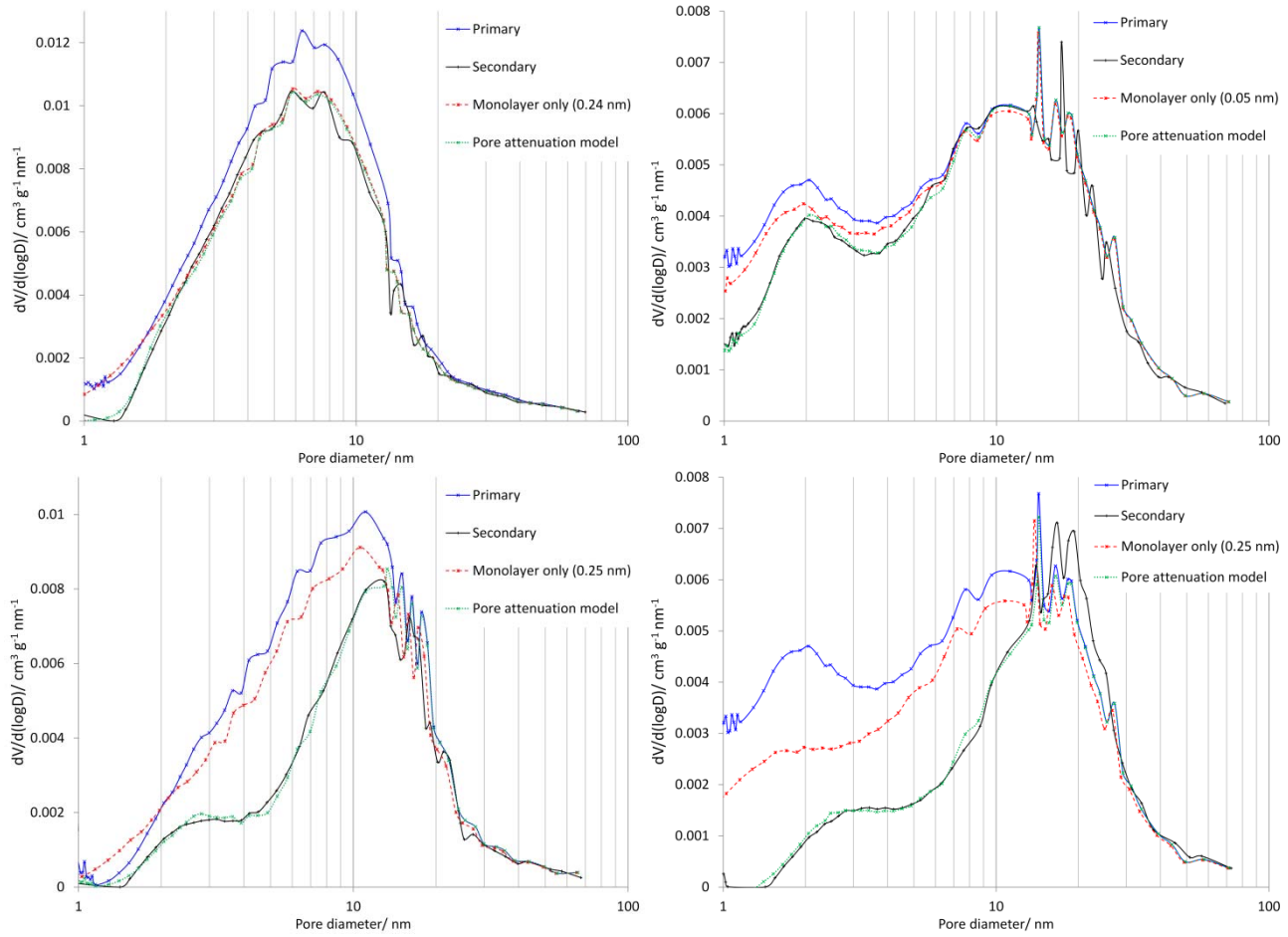


Figure S5: PSD curves of a) unimodal and b) bimodal aluminas after industrial fluorination, and c) unimodal and d) bimodal samples after laboratory fluorination with the pore attenuation/three zone model. These results supplement the material presented in Section 4.3 in the published manuscript. PSD curves are generated using the Halsey statistical thickness models.

Table S3: Fitting parameters for the models of pore attenuation in the studied aluminas (using the Halsey thickness model).

	Unimodal industrial	Bimodal industrial	Unimodal laboratory	Bimodal laboratory
<i>Three zone model parameter (unrestricted/kinetically restricted zones); c.f. eqtn (8)^a</i>				
$D_{kinetic}$	2.8	2.7	2.8	2.8
$\sigma_{kinetic}$	1	1	1.2	3
<i>Three zone model parameter (kinetically restricted/blocked pore zones); eqtn (20)</i>				
$D_{blocked}$	1.5	1.1	1.3	1.8
$\sigma_{blocked}$	0.2	0.6	1	0.7
<i>Pore attenuation model parameters; eqtn (16)</i>				
$A([HF])$	0.2	0.45	1.2	1.4
$D_{attenuated}$	1.5	1.1	1.3	1.5
$\sigma_{attenuated}$	0.8	3	6.2	6.2

^a References equations in the published manuscript

Section C. Rebinning Procedure for Monolayer Application in the ‘Monolayer/Three-Zone’ Model

As the BJH method discretizes the PSD by pore diameter, and the interval between pore diameters is not constant, shifting the monolayer-covered pore region to slightly smaller pores causes issues with rebinning pore length data, as described below. As a consequence, with pore lengths partitioned into the various regions, a new effective pore length distribution needs to be generated. This is done most easily by treating pore diameters and the new length regions as vectors. The i^{th} entry in a given pore length vector corresponds with the i^{th} entry a pore diameter vector D (D_i), and therefore when summing two length vectors the i^{th} entry is also assumed to be associated with the pore diameter D_i . Recombining the blocked and inaccessible regions is trivial; the inaccessible region vector is left unmodified, while all entries in the blocked region vector are set to zero, and the two vectors are simply added. Problems arise with the treatment of a monolayer; the value D_i is now modified to $D_i + 2t_m$ which does not, in general, corresponds with any entry in the vector D . To treat this, we have instead create a new vector D' which spans the entire range of pore sizes spanned by D , but with much finer detail (that is, there are many more discretized pores in the new model). We set the distance between each entry of D' equal to t_m/α ; the value α must be an integer, but can be varied, with larger values ensuring smoother fitting; we set the value at 300 in this work. New corresponding pore length vectors must also be created. For pores in the range $D_i \rightarrow D_{i+1}$, there are $\alpha(D_i - D_{i+1})/t_m$ entries in D' , and each entry is set at $L_i t_m / [\alpha(D_i - D_{i+1})]$; that is, the original length in this range is divided by the number of points in that interval, and this value is repeated over the span of this interval. This construction, though unwieldy, does ensure now that in the $D'_i \rightarrow D'_i + 2t_m$ transition there is an entry in D' that corresponds to the new pore value, namely the entry $D'_{i+2\alpha}$. Thus, to apply a monolayer to an original pore length distribution L , we construct the new longer vector L' , then set the first 2α entries to zero while shifting the entry L'_i to $L'_{i+2\alpha}$ (the final 2α values are generally dropped as they are now in out of the range of our analyses, anyway, which terminates at pores 1 nm in diameter). The L' vectors for the inaccessible and monolayer regions can now be added, and the values in this vector re-binned to correspond with entries in the original (shorter) pore diameter vector D .